Astron. Astrophys. 330, 97–107 (1998)

ASTRONOMY AND ASTROPHYSICS

COMPTEL observations of Centaurus A at MeV energies in the years 1991 to 1995

H. Steinle[1], K. Bennett[4], H. Bloemen[2], W. Collmar[1], R. Diehl[1], W. Hermsen[2], G.G. Lichti[1], D. Morris[3], V. Schönfelder[1], A.W. Strong[1], and O.R. Williams[4]

[1] Max-Planck-Institut für extraterrestrische Physik, Giessenbachstrasse, Postfach 1603, D-85740 Garching, Germany
[2] SRON-Utrecht, Sorbonnelaan 2, 3584 CA Utrecht, The Netherlands
[3] University of New Hampshire, Institute for Studies of Earth, Oceans and Space, Durham, NH 03824, USA
[4] Astrophysics Division, Space Science Departement of ESA/ESTEC, 2200 AG Noordwijk, The Netherlands

Received 24 July 1997 / Accepted 17 September 1997

Abstract. During the Compton Gamma-Ray Observatory (CGRO) observations made in Phase I, II, III, and IV/Cycle 4 in the years 1991 to 1995, the region on the sky including the radio galaxy Centaurus A was in the wide field-of-view of COMPTEL in 15 pointings of various durations.

The analysis of the COMPTEL data obtained during these 15 pointings shows emission consistent with the position of Cen A and we detected Cen A in two emission states (intermediate and low). Our data do not require, but also cannot rule out, that emission from a nearby X-ray source (MS1312.1-4221) contributes to the measured flux. But it is unlikely, that the high flux observed in the energy band 3 - 10 MeV during Phase II of the COMPTEL observations, is due to a significant contribution of this source.

The spectra in the COMPTEL energy range 0.75 - 30 MeV are consistent with the Centaurus A spectra in the energy range 0.05 - 4 MeV from OSSE and the 0.1 - 1 GeV data points from EGRET, both instruments also on board CGRO. The spectral form differs between the two observed emission states and we derive a γ-ray luminosity in the total energy band from 50 keV to 1 GeV of 5×10^{42} erg s^{-1} and 3×10^{42} erg s^{-1} for isotropical emission in the the intermediate and low emission state, respectively.

The inclusion of the contemporaneous OSSE and EGRET spectra stretches the covered energy range in this observations over almost five decades and puts hard constraints on models for the γ-ray emission of this AGN.

Key words: extragalactic astronomy – galaxies: active – BL Lacertae objects: individual: MS1312.1-4221 – galaxies: individual: Cen A – gamma-rays: observations

Send offprint requests to: H. Steinle (hcs@mpe-garching.mpg.de)

1. Introduction

Centaurus A (Cen A; NGC 5128; PKS 1322-427) is usually classified as a FR I type radio galaxy, as a Seyfert 2 object (Dermer & Gehrels 1995), and as a misdirected BL Lac type AGN (Morganti et al. 1992). It is one of the best examples of a radio-loud AGN viewed from the side ($\sim 70°$) of the jet axis (Ebneter & Balick 1983, Jones et al. 1996). Its proximity of ≤ 4 Mpc (Harris et al. 1984; Hui et al. 1993) makes it uniquely observable among such objects, even though its bolometric luminosity is not large by AGN standards. Cen A provides the opportunity to observe a misaligned AGN and a promising black-hole candidate in detail over the whole frequency range covered by the Compton Gamma-Ray Observatory (CGRO).

Radio observations revealed the huge lobes, which extend to an apparent diameter of 10° on the sky, optical observations showed filaments related to the inner jet seen in the radio and X-ray regimes, and X-ray observations detected flux variations on timescales of days. Cen A was one of the few known MeV γ-ray sources when the Compton Gamma-Ray Observatory was launched (Gehrels & Cheung 1992). Since then, it is among the objects which have been observed repeatedly by all CGRO instruments (Kinzer et al. 1995; Paciesas et al. 1993; Steinle et al. 1993; Thompson et al. 1995).

Historically, Cen A has exhibited greater than an order of magnitude X-ray intensity variability (see Bond et al. (1996) for a definition of the different emission states) with an intensity-independent spectral shape below about 100 keV. Most previous measurements, when fitted with models including a spectral break, show no distinct change of the spectral index ($\alpha \sim 1.7 - 1.8$) below the break (i.e. at lower energies than $\sim$ 100 keV) when the intensity changes (e.g. Baity et al. 1981, Feigelson et al. 1981, Morini et al. 1989, Maisack et al. 1992, Jourdain et al. 1993). Only one very early detection made during a short rocket flight (Lampton et al. 1972) measured a very hard X-ray spectrum with a power-law index of 1.0 . In γ-rays, Cen A has been observed in the past by various instruments and has been

found to exhibit states of high intensity as well (Bond et al. 1996, Kinzer et al. 1995, Steinle et al. 1993).

Very close ($\sim 2^\circ$) to the position of Centaurus A is, if one bears in mind the spatial resolution of most γ-ray telescopes, the BL Lac type object MS1312.1-4221. This object is also a pronounced X-ray (Arp 1994) and radio source (Stocke et al. 1990). It has once been proposed as a possible counterpart for the weak γ-ray source detected by EGRET from the Centaurus A region (Fichtel et al. 1994) or to be the reason for the extended appearance of the γ-ray contours in this region (Thompson et al. 1995). However, in a recent paper Nolan et al. (1996) state, that the high-energy emission detected by EGRET from this region, is more likely to be attributed to Cen A.

In this paper we report the results of the 15 observations made of the Centaurus A region in the 0.75 - 30 MeV range with the imaging Compton telescope COMPTEL on board CGRO (see Schönfelder et al. (1993) for a description of the instrument) between October 1991 and July 1995. To extend the energy range, we combine our data with simultaneous measurements made by OSSE (0.05 - 4 MeV) and EGRET (0.1 - 1 GeV) so that, in total, the spectra cover almost 5 decades in energy.

Section 2 contains what may be considered a very detailed description of the data analysis and the techniques employed. We felt it was necessary to describe this in such detail, as the measured fluxes are often close to the COMPTEL detection threshold. An understanding of the data reduction is required to provide confidence in these rather marginal results.

This paper is intended mainly to report on the results of the analysis of the COMPTEL data. Therefore the discussion concentrates on the interpretation of the results obtained, in the light of existing models and no attempt was made to develop new theoretical models for the γ-ray emission of Cen A. This, however, may be necessary and it is left to interested theorists.

Table 1. Observation journal of the Centaurus A region for Phases I, II, III, and IV/Cycle 4 of the CGRO observations

Obs.No. (VP)	start date (yy-mm-dd)	(TJD)	Δt (d)	D ($^\circ$)	t_e (d)
Phase I					
12.0	91-10-17	8546.6	14	3.0	4.4
14.0	91-11-14	8574.7	14	31.4	1.2
23.0	92-03-19	8700.6	14	20.5	1.5
27.0	92-04-28	8740.6	9	27.9	0.8
32.0	92-06-25	8798.6	7	23.8	0.7
Phase II					
207.0	93-01-12	8999.6	21	12.8	3.2
208.0	93-02-02	9020.6	7	2.4	1.5
215.0	93-04-01	9078.7	5	4.0	1.0
217.0	93-04-12	9089.6	8	4.0	1.7
Phase III					
314.0	94-01-03	9355.7	13	20.6	2.1
315.0	94-01-16	9368.7	7	20.6	1.0
316.0	94-01-23	9375.7	9	0.0	2.4
Phase IV / Cycle 4					
402.0	94-10-18	9643.6	7	24.4	0.8
402.5	94-10-25	9650.6	7	23.4	0.8
424.0	95-07-10	9908.6	15	3.0	3.9

(The Truncated Julian date is defined as TJD = JD - 2440000.5; for a description of columns 4, 5, and 6 see section 2.1)

2. Data

2.1. Observations

During the CGRO observation Phases I, II, III, and IV/Cycle 4, the Centaurus A region was in the wide field-of-view of COMPTEL in 15 pointings (Viewing Periods). A compilation of these observations is given in Table 1. Columns 1 to 3 of this table are self-explanatory. The fourth column (Δt) gives the duration of the whole observation in days. Column 5 (D) lists the distance of Cen A from the pointing direction of COMPTEL in degrees. The detector response of COMPTEL decreases almost linearly from a region of about 5° around the centre of the field-of-view (which is identical to the pointing direction) in which the instrument has its highest sensitivity, towards a distance from the pointing direction of about 50°, where the sensitivity drops below 10% (Schönfelder et al. 1993). Thus, observations in which the distance of the object from the pointing is more than $\sim 30^\circ$, are not used in this analysis. Column 6 (t_e) gives the effective observing time in days. This time is the net time in which Centaurus A was visible to the instrument. Several reasons exist which prevent measurements: Earth in the field-of-view, passage through the South Atlantic Anomaly where the instrument is switched off, data loss due to malfunction of tape recorders, or data loss during real-time telemetry in times where no ground station or relay satellite is avaliable. The effect of the decreasing detector response with distance from the pointing direction is also included in the effective observing time.

Viewing Period (VP) 14.0 was heavily influenced by the Earth in the field-of-view of COMPTEL, so that the effective observing time is rather poor. VP 23.0 suffered from the loss of data due to the malfunction of the tape recorders. After this observation, data were transmitted to ground in direct telemetry mode. The two short observations VP 215.0 and VP 217.0 from Phase II, which have an identical pointing and are separated by 6 days only, have been combined for the analysis (group "d"; see Table 2), and have not been analyzed individually.

2.2. Data analysis

The data analysis of all observations used in this paper has been made with the latest versions of the standard COMPASS (COMPTEL Processing and Analysis Software System; for a general description see den Herder et al. 1992). The analysis of the Centaurus A region in the field-of-view of the 15 observations was done in a consistent way using all γ-ray photons coming from a 60°-radius region centered on Cen A. All previously

analyzed and published observations have been re-analyzed to provide a self-consistent set of data.

All observations used for this paper to derive skymaps and flux values have been analyzed applying the Maximum-Entropy method (MEM) and the Maximum-Likelihood method (MLM), both described in more detail in the following sections. The results of both methods have been compared with each other and the error estimates have been cross-checked with the bootstrap method. However, the dominant uncertainty in these methods is caused by the high instrumental background. The structure of this background in the COMPTEL data space has to be known or approximated with very high accuracy (the source signal is only of the order of a few percent of the background!). Different approaches are possible and will be summarized in the sections below.

All data have been analyzed in the standard COMPTEL energy bands 0.75-1, 1-3, 3-10, and 10-30 MeV, and in the combined energy range 1 - 30 MeV to enhance statistics. In addition, groups of observations have been added together to increase statistics, if they have been made within a few months (see Table 2). This grouping of the data was also guided by the flux variations as measured in the 20 - 200 keV energy band by BATSE (Fig. 5), employing the earth-occultation technique (Paciesas et al. 1993). These BATSE data are publicly available through the BATSE World-Wide-Web site. COMPTEL measurements were combined only if the BATSE flux levels measured at the same time were of comparable value. This should avoid effects due to intensity-related spectral changes. Further, a data set of all observations except Viewing Period 12.0 was generated, as our observations were all made at about the same average intensity level except in VP 12.0, when the emission from the Cen A region was higher than in all following observations.

2.2.1. Maximum-Entropy maps

The first method usually applied to the COMPTEL data to obtain skymaps of the observed regions and to find sources of γ-ray emission, is the Maximum-Entropy method (MEM) which is described in full detail in Strong et al. (1992).

Deconvolution of the data with the MEM results in the "flattest" sky-map, i.e. a sky with the fewest possible sources consistent with the data. These resulting MEM skymaps give a first hint, whether an anticipated source is seen in an observation and whether additional sources of gamma radiation are present. Problems existed in the past with the flux determination of the detected sources, but this has been improved and the present software for MEM gives flux values consistent with all other methods. The all-sky maps of Strong et al. (1997) show Cen A clearly in the 1 - 3 and 3 - 10 MeV ranges, offset 20° from the intense Galactic plane diffuse emission.

2.2.2. Maximum-Likelihood maps

The next method usually applied to the COMPTEL data is the Maximum-Likelihood method (MLM). Here, for each pixel on the sky, a likelihood-ratio value ($-2\ln\lambda$) is calculated, which is a measure for the relative probability that a (point) source at this position (pixel) contributes to the measured data. Maxima in these maps indicate locations with a high probability for sources. The method is described in full detail in de Boer et al. (1992).

The value of the likelihood-ratio can be directly transformed into a significance for a detection, depending only on whether an unknown source is detected (three degrees of freedom; i.e. two coordinates and the flux) or a known source is seen (one degree of freedom; i.e. flux). For one degree of freedom, the significance of a detection follows a χ^2 distribution and is $\sqrt{-2\ln\lambda}$. The flux determination is also straightforward. Inaccuracies in the applied background model give systematic uncertainties in the significance and flux estimates. In the most recent application of MLM to COMPTEL data, the background modelling has been built in and is described in more general terms in the following section.

To identify an excess in the likelihood-ratio maps with a known object, the object has to lie within a certain distance of the excess. The closer the object is to a (local) maximum in the likelihood-ratio map, the higher is the probability for a positive identification. For this purpose, the so-called location-error contours are plotted in the likelihood maps. They specify the probability in σ that a source is located within the corresponding contours. The 1σ error contour is the innermost, enclosing the maximum in the likelihood map. The 2σ and 3σ contours have larger distances from the maximum. Around each (local) maximum they are derived by subtracting a certain value (which depends on the degrees of freedom) from the maximum. A candidate object has to be within the 3σ location-error contour to be accepted.

2.2.3. Background modelling

During a COMPTEL observation, typically more than 90% of the (potentially celestial) photons accepted on-board are from background, mainly instrumental. Thus a correct subtraction of the background is essential. Various methods to model the background for the COMPTEL observations have been developed and most of them have been implemented as options in the MEM and MLM analysis software.

Depending on the pointing of the instrument, a good background model for MEM may be averaged, smoothed observations of (source-free) regions at high galactic latitudes, or a smoothed averaged combination of other source-free regions of the sky. Cen A is 50° off the galactic centre at a galactic latitude of +19° and thus the high latitude background seems to be a good choice. However, the instrumental background exhibits long term variations in spectral shape and intensity, and as a function of the satellite position in orbit, complicating the analysis. This variability of the background is the main reason why the single viewing periods have been analyzed individually before they have been combined for further analysis.

The MLM has the possibility to internally adjust the telescope response to the presence of sources and generate a background model which includes this sources. The background in this case is directly derived from the data by a smoothing pro-

Table 2. Measured photon fluxes (in units of 10^{-5}cm^{-2}s^{-1}) and 2σ upper flux limits for Centaurus A in all five COMPTEL energy bins.

Obs.No.	Group	Energy Band (MeV)					$-2\ln\lambda$ *
(VP)		0.75 - 1	1 - 3	3 - 10	10 - 30	1 - 30	(1 - 30 MeV)
Phase I							
12.0	a	16.4 ± 8.1	< 17.6	4.0 ± 2.4	1.6 ± 0.8	18.4 ± 6.5	8.8
14.0	a	31.0 ± 11.7	16.4 ± 10.9	< 9.2	< 5.8	< 28.5	0.2
23.0	b	16.8 ± 15.7	< 28.6	< 15.8	< 2.9	< 39.0	0.7
27.0	b	< 20.1	30.3 ± 12.6	7.1 ± 6.2	< 3.9	28.3 ± 13.3	5.0
32.0	b	< 20.5	< 35.0	< 14.9	< 5.7	15.1 ± 13.5	1.4
group a		22.6 ± 6.7	9.1 ± 5.6	< 4.9	1.1 ± 0.7	12.3 ± 5.7	5.1
group b		7.7 ± 6.1	8.8 ± 5.3	2.2 ± 2.1	0.8 ± 0.7	22.4 ± 5.4	19.0
all except VP12		< 18.8	13.5 ± 6.2	< 7.9	< 1.9	17.1 ± 6.5	7.5
all Phase I		14.1 ± 5.2	10.8 ± 4.5	2.2 ± 1.9	< 1.4	16.3 ± 4.6	13.6
Phase II							
207.0	c	< 12.2	< 14.3	8.8 ± 2.6	1.3 ± 0.9	20.6 ± 6.7	10.4
208.0	c	18.8 ± 14.8	14.5 ± 12.0	5.1 ± 4.4	< 3.8	25.2 ± 12.0	4.9
group c		< 11.0	< 15.7	8.0 ± 2.3	< 1.8	23.3 ± 5.9	17.3
215.0+217.0	d	< 23.3	21.3 ± 8.3	10.8 ± 3.1	< 1.7	33.2 ± 8.3	17.8
all Phase II		< 11.9	5.8 ± 4.6	8.6 ± 1.8	< 1.7	25.5 ± 4.8	31.0
Phase III							
314.0		28.1 ± 9.9	< 26.6	< 6.7	2.3 ± 1.4	< 19.5	0.0
315.0		< 6.9	4.5 ± 2.9	< 2.2	< 2.4	< 8.1	0.6
316.0		< 30.6	< 17.1	< 9.0	< 1.6	< 22.8	0.2
all Phase III		24.1 ± 6.2	< 14.9	< 3.9	< 1.2	< 9.5	0.0
Phase IV/Cycle 4							
402.0	e	18.7 ± 14.2	< 36.1	< 9.1	< 3.0	< 27.5	0.0
402.5	e	< 28.7	26.6 ± 12.1	< 8.9	< 4.2	< 29.8	0.1
424.0		< 13.5	18.6 ± 7.7	3.6 ± 2.7	< 1.3	22.9 ± 7.6	10.0
group e		9.7 ± 9.5	18.6 ± 8.9	< 6.4	< 2.2	< 18.7	0.0
all Phase IV		< 15.2	21.9 ± 5.8	< 4.5	< 1.1	18.0 ± 5.9	10.3
all except VP 12		8.5 ± 3.2	10.4 ± 2.8	2.3 ± 1.1	< 0.6	10.5 ± 2.8	15.4
all observations		9.1 ± 3.0	6.4 ± 2.5	2.1 ± 1.0	< 0.6	9.6 ± 2.6	15.3

* the significance in the total 1 - 30 MeV energy band for a source at the position of Cen A is $\sqrt{-2\ln\lambda}$

cess which suppresses signals from point sources to obtain a source-free background. Bloemen et al. (1994) have described this in detail. The resulting background model can be used by other methods as well, and such a MLM background model has been used in the MEM analysis.

Other methods for the background estimation use the symmetry of the COMPTEL instrument to define regions in the field-of-view with identical observation conditions (in the same observation) to be used as source or background fields. But the loss of some detector elements due to photomultiplier failures make the application of these methods more and more difficult.

2.2.4. Determination of fluxes

The photon fluxes in Table 2 are calculated from the measured source counts in the MLM maps, taking into account the detector response and the effective observing time. The inclusion of known strong sources and the diffuse emission of the Galaxy into the background model is, if they are present in the field-of-view, also necessary to derive correct fluxes.

For a known source, the flux is determined at the known position of the object. If a "new" source is detected, fluxes will be determined at the maximum position in the likelihood maps. As already mentioned above, the derived flux values always have been cross checked with bootstrapping and the fluxes derived with the Maximum-Entropy method.

2.2.5. Error estimates

All quoted flux errors are 1σ statistical errors which include corrections for live-time effects and the loss of events due to the applied time-of-flight window in the onboard background suppression method. The derived errors from the MEM have been verified by testing the distribution of the calculated flux values using the bootstrap method (Simpson & Mayer-Hasselwander 1986). In this bootstrap method, many sub-samples (in our anal-

ysis for this paper we have usually generated $\sim$ 100) of the whole data were choosen randomly and MEM maps were generated. The resulting distributions of the locations and fluxes have been checked to be in agreement with what was expected from the originally derived errors. In the case of MLM Monte Carlo simulations were made to verify the error estimates.

To take into account our best estimate of any systematic errors still contained in the results, 30% has to be added to the errors given.

The 1σ errors for the parameters of the model fits to the measured spectra have been calculated according to the rules given in Lampton et al. (1976).

2.2.6. Upper limits

If a source is detected, all measurements with a source flux $> 1\sigma$ are given as datapoints with the relevant error. If the source flux is less than the calculated 1σ error, a 2σ upper limit for this measurement is given. This 2σ upper limit is derived by adding twice the 1σ error flux to the source flux. If the calculated source flux is negative (due to the statistical fluctuations and the background subtraction), the 2σ errors are added to zero flux.

3. Results

The analysis of the COMPTEL data obtained from the Centaurus A region during Phases I, II, III, and IV/Cycle 4, gives the following results.

3.1. Location

COMPTEL is an imaging instrument and can locate the position on the sky of a source emitting γ-rays in the MeV range. Depending on the strength of the source, the location accuracy varies between $\sim 1^\circ$ for strong sources and few degrees for weaker sources. As described in Schönfelder et al. (1993), only strong sources with a separation $\gtrsim 4^\circ$ can be resolved.

Because of the limited statistics in the single observations in the standard energy bands, we also used the wider energy band 1 - 30 MeV and added observations to determine a more exact location of the emission from the Cen A region. It has to be pointed out, that for the purpose of locating a source, this is valid, as time variations are not critical if the source is always present in the data. This is the case in our observations. Also, it has to be mentioned, that it is an intrinsic feature of the background dominated wide-field-of-view instrument COMPTEL, that adding many observations, does not necessarily improve the detection significance, as different background areas and different orientations of the spacecraft may enhance the background and thus reduce the sensitivity.

The most significant signal from the Cen A region, with a maximum likelihood-ratio value ($-2\ln\lambda$) of 31 at the position of Cen A[1], was obtained during Phase II in the energy band 1 - 30 MeV. Figure 1 shows a map of this data in an area of $30^\circ \times 30^\circ$ around Centaurus A. The position of Cen A coincides with the maximum in the likelihood-ratio.

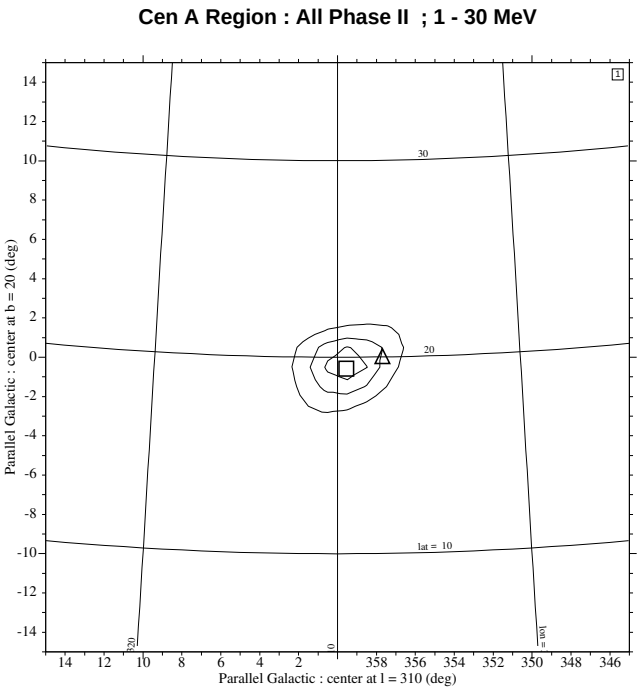

Fig. 1. COMPTEL location contours for 1 - 30 MeV emission, obtained from a combination of all Phase II observations of the Centaurus A region . The positions of Cen A and MS1312.1-4221 are marked by a square and a triangle, respectively. The 1σ, 2σ, and 3σ location-error contours are plotted around the maximum of $-2\ln\lambda = 31$ which coincides with Cen A. The coordinate grid is in galactic coordinates. Note the large area covered ($30^\circ \times 30^\circ$) and the lack of other sources of comparable strength.

As mentioned above, the total of all observations does not necessarily give a larger significance and hence a better location. As it is seen in Fig. 2, the likelihood-ratio value ($-2\ln\lambda$) is "only" 15.3 at the position of Centaurus A in the energy band 1 - 30 MeV, when all observations are added together. But Cen A is still within the 1σ location contour.

The location contours in the COMPTEL skymaps for the other observations of the Centaurus A region are always compatible with an origin of the emission from Cen A. However, the BL Lac type object MS1312.1-4221 (Stocke et al. 1990) which is only $\sim 2^\circ$ away from Cen A, often has about the same or sometimes even slightly higher probability for being the source of emission than Cen A, due to the large error region. From our data it cannot be ruled out, that MS1312.1-4221 may contribute to the emission from this region. However, observations with the SIGMA telescope (Bond et al. 1996) which has a good angular resolution, show no emission in the energy band 40 - 120 keV at the position of MS1312.1-4221 during their observations, which overlap in time with the CGRO observations. Also, during Phase II, when we measured the strongest emission from the Cen A region, the maximum in the likelihood-ratio lies ex-

[1] Throughout this paper we refer to the (radio) nucleus of Centaurus A when we address the position of this object.

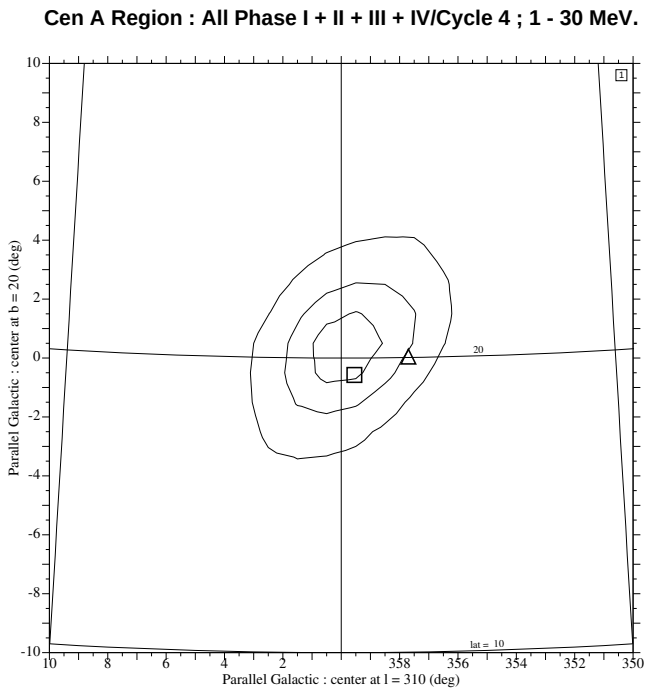

Fig. 2. COMPTEL location contours for 1 - 30 MeV emission, obtained from the combination of all observations of the Centaurus A region. The positions of Cen A and MS1312.1-4221 are marked by a square and a triangle, respectively. The 1σ, 2σ, and 3σ location-error contours are plotted around the maximum of $-2\ln\lambda = 16.8$. The likelihood-ratio value at the position of Cen A is 15.3 . The coordinate grid is in galactic coordinates and the area shown is $20^\circ \times 20^\circ$.

actly at the position of Cen A and MS1312.1-4221 lies outside the 2σ contour (Fig. 1).

No significant emission from other parts of the Cen A system has been detected with COMPTEL. As it can be seen from Figs. 1 and 2, which show an area large enough to cover the giant outer radio lobes, the only emission detected comes from the direction coinciding with the nucleus of the galaxy. If γ-rays with comparable intensity would be emitted from the outer radio lobes, COMPTEL would be able to resolve the different origins.

3.2. Spectra

Centaurus A is known to be variable on time scales of days to months in all wavelength bands (see Sect. 3.4.). Therefore, to derive meaningful spectra, a compromise had to be found between the need to add observations to improve statistics and the risk of averaging out variations, by adding observations which are separated by too large a time span. Under this consideration, and by using the BATSE light curve shown in Fig. 5 to select data from similar emission states assuming that they are somehow related to the spectra (see below), we have added only observations which were separated by not more than few months. The resulting groups of observations (a - e) are marked in the second column of Table 2 and the measured flux values for these groups are listed in the same table. A special case (all observations except VP 12.0) for comparison with OSSE was added as well.

Table 3. Fit-parameter values for a single power-law model ($I_0 \times E^{-\alpha}$; E in MeV, I_0 in units of 10^{-5} cm^{-2} s^{-1} MeV^{-1}) derived from the COMPTEL observations of the Centaurus A region with more than two data points. For comparison, the high-energy part of the broken power-law fit to the simultaneous OSSE observation in viewing period 12.0 and to the sum of all other OSSE observations of Cen A in Phases I to III are also listed (Kinzer et al. 1995).

Observation	I_0	α	reduced χ^2
VP 12.0	37^{+35}_{-33}	$2.3^{+0.6}_{-0.9}$	1.1
VP 208.0	30^{+47}_{-28}	$2.3^{+4.0}_{-1.1}$	0.2
group a	46^{+20}_{-21}	$4.6^{+3.9}_{-1.5}$	1.2
group b	15^{+18}_{-12}	$2.2^{+1.9}_{-0.8}$	0.2
all Phase I	31^{+17}_{-16}	$3.2^{+1.7}_{-1.0}$	0.3
all but VP 12.0	$21^{+\ 9}_{-\ 9}$	$2.6^{+0.8}_{-0.6}$	0.2
sum of all obs.	$18^{+10}_{-\ 9}$	$2.9^{+1.5}_{-0.6}$	1.2
OSSE VP 12.0	32.0 ± 1.4	2.3 ± 0.1	
all other OSSE	32.9 ± 1.4	2.0 ± 0.1	

An attempt to fit a model to the spectrum of an observation (or a combination of observations) has only been made if at least three data points with significances $\geq 1\sigma$ have been measured. Thus, fits were made only in seven cases: Viewing Periods 12.0 and 208.0, observation groups a and b, for the average spectra over a much wider time span of Phase I, all observations together, and for the combination of all observations except VP 12.0. Due to the small number of data points, only single power-law models have been used and the resulting fit-parameter values for a model of the form $I_0 \times E^{-\alpha}$ are given in Table 3 for all seven spectra. In addition, the two OSSE fits to VP 12.0 and the sum of all other OSSE observations of Cen A as given in Kinzer et al. (1995) are listed.

Of special interest are of course the viewing periods in which OSSE and EGRET observed Centaurus A simultaneously with COMPTEL, so that data over a much wider energy range are available. Simultaneous observations with OSSE have been made in Viewing Periods 12.0, 215.0, 217.0, 316.0, and 424.0 . EGRET always views the same sky region as COMPTEL and has been active during the entire time interval covered by this paper.

3.2.1. Intermediate emission state spectrum

The longest simultaneous observation occured in Viewing Period 12.0, when, for two weeks, Cen A was also observed by the OSSE instrument (Kinzer et al. 1995). This is the only simultaneous single observation, for which the OSSE and EGRET data have been published so far and it is the only observation, in which Cen A was in an intermediate emission state.

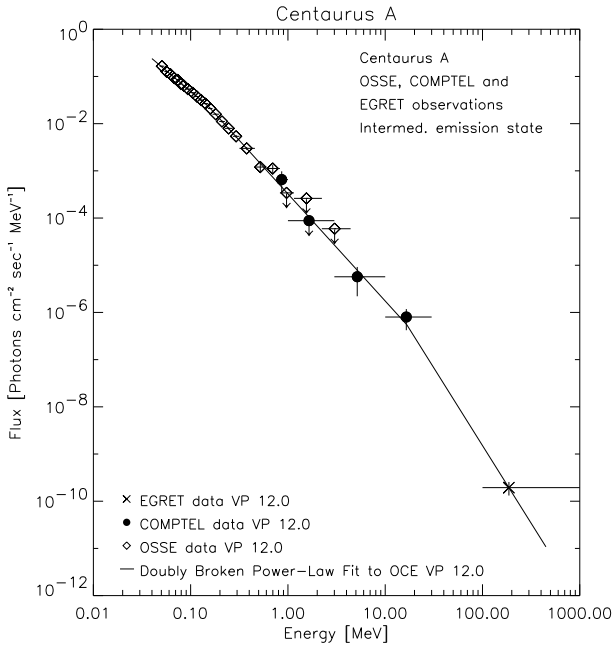

Fig. 3. Combined spectrum from Centaurus A as measured by OSSE (0.05 - 4 MeV), COMPTEL (0.75 - 30 MeV), and EGRET (0.1 - 1 GeV) simultaneously during Viewing Period 12.0 (intermediate emission state). The solid line is the doubly broken power-law fit to the combined data. The broken power-law fit given in Kinzer et al. (1995) for the OSSE data alone, is indistinguishable from the fit shown here.

The OSSE spectrum connects very smoothly with the COMPTEL data in the overlapping region around 1 MeV (Fig. 3). The extrapolation of the broken power-law spectral fit to the OSSE data (0.05 - 1 MeV), which has a spectral index of $\alpha = 2.3$ above the break energy of 150 keV (Kinzer et al. 1995), also fits extremely well to the COMPTEL data. Indeed, it is almost identical to the fit to the COMPTEL data alone.

The simultaneously measured EGRET data point (Thompson et al. 1995) lies below the extrapolation of the fit to the COMPTEL data and requires an additional break in the power-law spectrum.

The combined OSSE, COMPTEL and EGRET data span almost five decades of energy. The model fit to the combined data, which is shown in Fig. 3, is a doubly broken power-law of the form

$I_1 \times (E/E_{b_1})^{-\alpha_1}$ for $E < E_{b_1}$,
$I_1 \times (E/E_{b_1})^{-\alpha_2}$ for $E_{b_1} \leq E < E_{b_2}$,
and
$I_2 \times (E/E_{b_2})^{-\alpha_3}$ for $E \geq E_{b_2}$

(E_{b_1} and E_{b_2} are the break energies in MeV).
The resulting parameters are :

$I_1 = \left(2.4^{+0.6}_{-0.6}\right) \times 10^{-2}$ [photons cm^{-2} s^{-1} MeV^{-1}] ,
$I_2 = \left(5.4^{+24.8}_{-4.6}\right) \times 10^{-7}$ [photons cm^{-2} s^{-1} MeV^{-1}] ,
$E_{b_1} = 0.15^{+0.03}_{-0.02}$ [MeV] ,
$E_{b_2} = 16.7^{+27.8}_{-16.3}$ [MeV] ,
$\alpha_1 = 1.74^{+0.05}_{-0.06}$,
$\alpha_2 = 2.3^{+0.1}_{-0.1}$,
$\alpha_3 = 3.3^{+0.7}_{-0.6}$.

3.2.2. Low emission state spectrum

Except for Viewing Period 12.0, all COMPTEL (and EGRET) observations were made when Cen A was in a low emission state. This can be seen in Fig. 5, where the BATSE monitor data are plotted and the COMPTEL observation periods are indicated. Although during the whole Phase I (TJD 8392 - 8942) the flux as measured with BATSE was declining from an intermediate state to the low emission state, the COMPTEL observations fall always into the minima of the light curve during this period and thus are representative of the low emission state.

For these low emission state observations, no simultaneous single observations have been published by other CGRO instruments. This is due to the fact, that for a significant signal, several observations have had to be combined. Thus, although all OSSE (except VP 43.0) and EGRET observations have been made simultaneously with COMPTEL, no consistent set of simultaneous low emission state observations is available. On the other hand, all observations have been made when Cen A was in a low state, and so we assume, that all those observations can indeed be compared.

The low emission state spectrum shown in Fig. 4 was derived by combining the following observations :

- the OSSE data are the sum of Viewing Periods 43.0, 215.0, 217.0 and 316.0 (Kinzer et al. 1995); only the fits are plotted for clarity
- the COMPTEL data are all observations (see Table 1) except Viewing Period 12.0
- the EGRET data point is from the Phase II observations only (Thompson et al. 1995)

The COMPTEL data points are consistent with the OSSE measurements in the overlapping region around 1 MeV and lie between the two possible extrapolations of the OSSE spectrum: a broken power-law (dashed line in Fig. 4; power-law index $\alpha = 2.3 \pm 0.1$) or a power-law with exponential cut-off at higher energies (dash - dotted line in Fig. 4). The extrapolation of the fit to the COMPTEL data alone (dotted line) towards higher energies, exactly matches the EGRET data point. The combination of all data available from 50 keV to 1 GeV results in the following fit

$I_1 \times (E/E_{b_1})^{-\alpha_1}$ for $E \leq E_{b_1}$,
$I_1 \times (E/E_{b_1})^{-\alpha_2}$ for $E_{b_1} < E \leq E_{b_2}$,
and
$I_2 \times E^{-\alpha_3}$ for $E > E_{b_2}$

(E_{b_1} and E_{b_2} are the break energies in MeV).
The resulting parameters are :

$I_1 = \left(1.4^{+0.6}_{-0.6}\right) \times 10^{-2}$ [photons cm^{-2} s^{-1} MeV^{-1}] ,
$I_2 = \left(2.1^{+0.9}_{-0.9}\right) \times 10^{-4}$ [photons cm^{-2} s^{-1} MeV^{-1}] ,

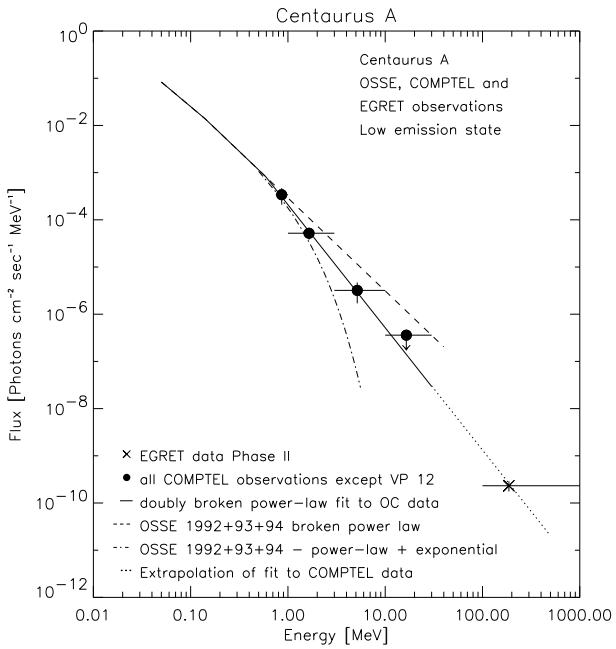

Fig. 4. Combined spectrum from Centaurus A as measured by OSSE (0.05 - 4 MeV), COMPTEL (0.75 - 30 MeV), and EGRET (0.1 - 1 GeV) during the low emission state. The solid line is the doubly broken power-law fit to the combined data of OSSE and COMPTEL. The EGRET data point (Thompson et al. 1995) lies exactly on the extrapolation (dotted line) of the COMPTEL fit. Two possible fits (Kinzer et al. 1995) to the OSSE data are also shown. See text for more details.

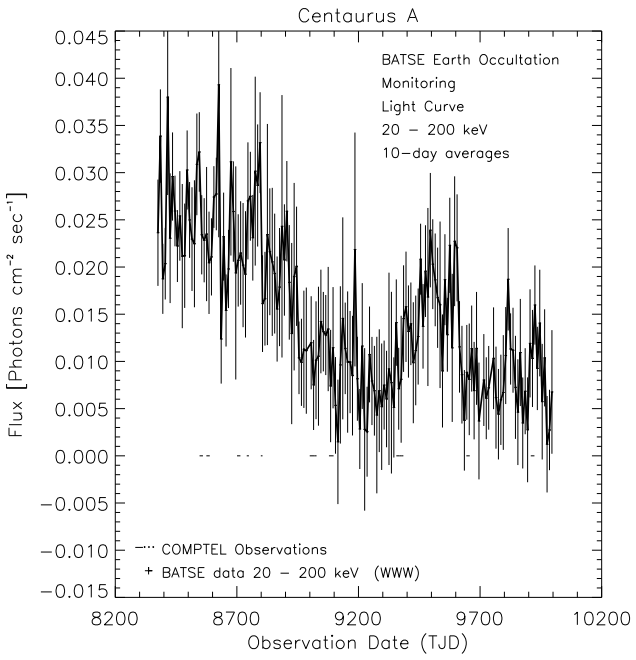

Fig. 5. Light curve of Centaurus A in the energy band 20 - 200 keV as observed by BATSE covering Phases I to IV/Cycle 4 in the years 1991 to 1995 (BATSE public data (WWW)). The data have been averaged over 10-day intervals. The 15 COMPTEL observation periods are indicated at the 0.0 flux level.

$$E_{b_1} = 0.14^{+0.03}_{-0.03} \quad [\mathrm{MeV}] ,$$
$$E_{b_2} = 0.59^{+0.02}_{-0.02} \quad [\mathrm{MeV}] ,$$
$$\alpha_1 = 1.73^{+0.05}_{-0.05} ,$$
$$\alpha_2 = 2.0^{+0.1}_{-0.1} ,$$
$$\alpha_3 = 2.6^{+0.8}_{-0.6} .$$

3.3. Gamma-ray luminosity

From the spectra of the combined OSSE, COMPTEL and EGRET data, the γ-ray luminosity (50 keV to 1 GeV) can be derived for the two emission states. Assuming a distance of 3.5 Mpc (H_0 = 50 km s^{-1} Mpc^{-1}; z = 0.0006; q_0 = 0.5) and an isotropically emitting source, we derive

$$L^{\mathrm{m}}_{\gamma} = 5 \times 10^{42} \text{ erg s}^{-1}$$
$$L^{\mathrm{l}}_{\gamma} = 3 \times 10^{42} \text{ erg s}^{-1}$$

for the intermediate and low emission state, respectively.

3.4. Variability

Variability is one of the well-known features of Centaurus A and is observed in all wavelength regimes from radio to γ-rays (Abraham et al. 1982 (radio), Terrell 1986 (X-ray), Bond et al. 1996 (hard X-ray), Kinzer et al. 1995 (γ-ray)).

All our observations except Viewing Period 12.0 were made when Cen A was in a low emission state in hard X-rays as defined in Bond et al. (1996) as it is obvious from the hard X-ray light curve measured by BATSE during the time interval covered by our observations (Fig. 5). No CGRO observations have been made in the (ultra-) high emission states described in Bond et al. (1996) since Cen A has not exhibited such a high emission since the launch of CGRO. Only during the first observation phase of CGRO, was Cen A in an intermediate intensity state. From Fig. 5 it is obvious, that at least three different time scales of variability exist in the 10-day averages: short-term "flickering" on time scales of tens of days, medium-duration variations lasting about a year, and long-term variations stretching over several years.

3.4.1. Variability in global flux

Although we have five observations in Phase I, Cen A was only during VP 12.0 in a higher (intermediate) intensity state. The other four fell in periods of low intensity as did all other following observations. Variability is present in our data, although due to the limited statistics, only crude statements can be made and no time resolution within a single observation is possible.

On short time scales, the largest flux variation between adjacent observations occured in the energy band 0.75 - 1 MeV in Phase III between Viewing Periods 314.0 and 315.0 (see Table 2). Both observations are separated by $\sim$ 10 days and the drop in the intensity is more than 2σ.

The largest variation observed is in the total energy band 1 - 30 MeV between Phase II and Phase III, where the flux drops by more than 3.3σ (see Table 2). The time interval between those

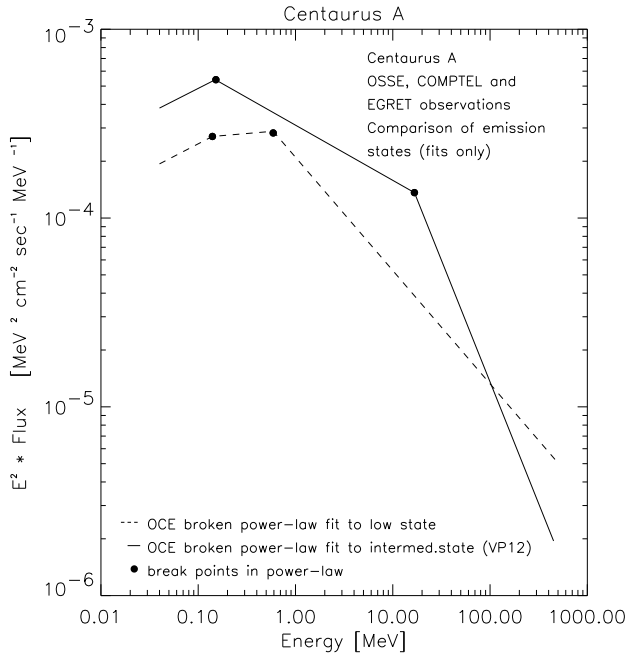

Fig. 6. $E^2\times$ Flux spectrum from Centaurus A from the combined OSSE, COMPTEL and EGRET mesurements in the intermediate (solid line) and low emission state (dashed line). The breaks in the double broken power-law model fits to the data are highlighted by the large dots.

observations is about one year. However, as described in more detail in the following section, the flux in the total energy band 1 - 30 MeV may be strongly influenced by the high intensity measured in the 3 - 10 MeV band. Also, as can be seen from Table 2, the flux below 1 MeV shows the opposite behaviour, but the significance is marginal in this case.

3.4.2. Variability in the 3 - 10 MeV energy band

It is obvious from Table 2, that a strong enhancement (actually the most significant emission of all measurements) in the 3 - 10 MeV energy band was observed during Phase II. This strong enhancement in this energy band was seen in three of the four Phase II observations and the fourth measurement also detects emission in this energy band although with less significance. Unfortunately, at present no satisfactory resolved energy spectrum in this 3 - 10 MeV energy band can be derived from the COMPTEL data as the total signal is only about 5σ and no finer energy resolution with sufficient statistics can be achieved. A detailed search for possible strong emission lines, as e.g. for the 4.5 MeV line (from excited ^{12}C) reported by Hall et al. (1976) is thus prohibited.

3.4.3. Variability in the overall spectra

Variations are also suggested in the power-law indices of the seven derived COMPTEL spectra for which a model fit to the data was possible (see Table 3), and in the spectra of the two emission states observed.

Compared to the intermediate spectrum of Viewing Period 12.0, we find that the single spectra in the COMPTEL energy range 0.75 - 30 MeV measured in the low state are, in almost all cases, steeper (Table 3). Also the power-law index of the sum of all (low state) observations except VP 12.0 has a marginally softer spectrum in the COMPTEL energy range.

However, when the spectra of Cen A from the combined observations of OSSE, COMPTEL and EGRET are plotted (Fig. 6), which cover the enery range from 50 keV to 1 GeV, the low state spectrum turns out to be harder (flatter) and the intermediate state spectrum is softer (steeper) in the high-energy part. This seeming discrepancy is mainly due to the shift of the second break in the double power-law fit from the high-energy end to the low-energy end of the COMPTEL energy range.

4. Discussion

The identification of the emission detected by COMPTEL from the Centaurus A region with the active galaxy Cen A is made plausible by two main arguments - the positional agreement of our data with this source, and the excellent agreement of our spectra with the simultaneous measured OSSE spectra.

Several detections of Cen A in the hard X-ray and γ-ray range have been reported in the past, but it has to be pointed out, that all have been made by instruments which had, like COMPTEL, a rather poor angular resolution of several degrees (for references see von Ballmoos et al. 1987). They are unable to distinguish between two possible candidate objects for the measured emission: Cen A and the BL Lac type object MS1312.1-4221, separated by 2° from each other. Only the SIGMA experiment (Jourdain et al. 1993) has the capability to really separate the two sources and Cen A is the only source seen at hard X-rays. Our data, although they cannot exclude a contribution of MS1312.1-4221 to the emission of the region, do not require it. Cen A is clearly the object always consistent with the data, and in our most significant measurement, Cen A coincides with the maximum in the likelihood map (Fig. 1). OSSE has a limited capability to define the possible contribution of the BL Lac object to the emission they observed. Again, an additional emission is not required, but if present, its contribution is 10% maximum (Kinzer private communication).

The other point in favour of Cen A is the excellent agreement of the OSSE spectrum with our data in the transition region around 1 MeV. When the OSSE VP 12.0 high-energy part of the broken power-law fit is extrapolated up to 30 MeV, it perfectly falls on the power-law fit to the COMPTEL VP 12.0 data alone. Also, if both data sets are fitted together, the resulting fit is identical to the OSSE fit alone (Fig. 3). In the low emission state, the COMPTEL data again smoothly connect to the OSSE data and the COMPTEL spectrum lies between the extrapolation of the two equally good fits to the OSSE data (Fig. 4). The comparison of the spectra of both emission states strongly suggests that the emission measured by OSSE and COMPTEL comes from the same source. Similarly, the perfect match of the extrapolation of the COMPTEL spectrum with the EGRET data point for the low emission state, and the plausible steepening of the spectrum

between the COMPTEL and EGRET energies in the intermediate emission state in VP 12.0, strengthen the identification of the EGRET source with Centaurus A.

Detections of emission from Cen A reported in the past indicated large variations in spectral shape. However, the hard X-ray and γ-ray spectral variability correlated with the intensity seems to exist only above $\sim$ 100 keV. Most previous measurements, when fitted with models including a spectral break, show no distinct change of the spectral index below the break (i.e. at lower energies) when the intensity changes (e.g. Baity et al. 1981, Feigelson et al. 1981, Morini et al. 1989, Maisack et al. 1992, Jourdain et al. 1993). Distinct changes in the spectral shape above $\sim$ 100 keV correlated with the intensity have recently been found by OSSE (Kinzer et al. 1995). Our new results confirm this correlation of the spectral behaviour above $\sim$ 100 keV for the low and intermediate emission states and show, that this correlation is present up into the GeV regime. Observations of Cen A at intensity levels approaching the historically highest observed state would provide greatly improved observation precision and would enable further tests of hypotheses concerning intensity-dependent spectral evolution which were advanced to explain the low and intermediate intensity level observations made so far (Kinzer et al. 1995).

The combination of the OSSE, COMPTEL and EGRET data of the first Viewing Period 12.0, gives a simultaneous measured spectrum which covers almost 5 decades in energy. The measured emission extends up to 1 GeV and a gradual steepening of the spectrum is observed in this energy range. Thus Compton reflection models for the γ-ray emission like in Skibo et al. (1994) (using only OSSE data) become very unlikely, as unrealistic model parameters have to be assumed to obtain scatter angles (especially for the high energy γ-ray photons) which are comparable to the viewing angles derived by other methods. The spectra from Cen A show interesting similarities with jet-aligned blazars (McNaron-Brown et al. 1995), and in particular with the well-studied quasar 3C273 (Johnson et al. 1995, Lichti et al. 1995). Both show spectral breaks in the soft γ-ray regime, and both have intensity-independent power-law shapes below the break (at lower X-ray energies). The principal difference is the energy and magnitude of the break(s) and the maximum of the emission. These two AGNs may be fundamentally similar, with the principal differences arising from the different jet-viewing angle, as suggested by Dermer & Schlickeiser (1993). The inverse Compton model for Blazar emission from Marcowith et al. (1995) also allows γ-ray emission of the right magnitude to be scattered onto the observed large viewing angle. The ratio they predict for the difference in luminosity between "on-(jet)axis" and from the side is of the order of 10^4. This would place Cen A among the weaker Blazars if seen "on-axis". In addition, our results seem to contradict the assumption (see Gehrels & Cheung 1992 for a review), that the energy output of Centaurus A per decade of photon energy peaks in the MeV region (see Fig. 6). The maximum lies between 150 and 600 keV depending on the emission state and it would be very interesting to see, whether this observed shift of the peak position towards lower energies also is true in a real high state. The model of Marcowith et al. (1995) predicts such a spectral break around 150 keV in the case of system parameters like the ones of Cen A. In the light of unified models for AGN (Antonucci 1993, Urry & Padovani 1995) it is interesting to note, that if Cen A is not a very special case in the class of AGN viewed from the side, this class may contribute significantly to the extragalactic background at energies immediately below 1 MeV. Because of the large number of AGN we naturally view from an angle somewhere between the extreme cases of viewing along the jet axis (Blazars) and perpendicular to it (Seyferts), and due to the fact that they, like Cen A, may have their maximum of emission just below 1 MeV, their contribution to the cosmic background at these energies will not be negligible.

The strong enhancement of the emission in the 3 - 10 MeV energy band seen in the Phase II observations, of course suggests that this may be a hint of line emission during this time. Hall et al. (1976) had observed enhanced emission at 4.5 MeV and they attributed this emission to a nuclear line from excited ^{12}C. Since then, several experiments (for a review see von Ballmoos et al. 1987) had searched for this line, but only upper limits could be derived. A blob of metal-rich material which moves through the jet could produce such temporary (line) emission. Given the low satistics (even in these significant Phase II detections), no detailed spectral analysis within the COMPTEL energy bands is possible for these observations. Therefore it is unclear at this time, whether the strong excess in the COMPTEL 3 - 10 MeV band is due to unresolved line emission.

Variability on all time scales is one of the well-known properties of Centaurus A. But due to the limited statistics of our instrument, the only new results on this topic obtained by us worth addressing here, are the indications for changing spectra which are connected to the intensity as discussed above, and the change in the γ-ray luminosity (calculated for isotropic emission) between the two observed intensity levels. This luminosity in the energy interval 50 keV to 1 GeV changes by about a factor 2 between the two observed emission states from $L_\gamma^{\rm m} = 5 \times 10^{42}$ erg s^{-1} to $L_\gamma^{\rm l} = 3 \times 10^{42}$ erg s^{-1} in the intermediate and low emission state, respectively. Such changes in the luminosity are common, and often much larger, in all known objects of the AGN family. In comparison to other AGN, Cen A is a weak source and the derived luminosities are upper limits to the real emission. However, this upper limits derived assuming isotropic emission for a source which is viewed from the side of the jets, may be more realistic than values derived from a highly beamed source, which the observer views along the jet. Cen A is so well detected only because it is so close. What the γ-ray luminosity is in the real high emission state may yet be seen, if future CGRO measurements are made during such a bright state.

Acknowledgements. This research was supported by the Bundesministerium für Forschung und Technologie under the grant 50 QV 9096, by NASA contract NAS5-26645 and by The Netherland's Organization for Scientific Research (NWO). We thank Bob Kinzer (NRL) for providing us with the OSSE data of Viewing Period 12.0 . The use of the public BATSE occultation data on Cen A at the WWW site *"http://cossc.gsfc.nasa.gov/cossc/batse/hilev/occ.html"* is acknowledged gratefully.

References

Abraham Z., Kaufmann P., Botti L.C.L., 1982, AJ 87, 532-536

Antonucci R., 1993, ARA&A 31, 473-521

Arp H., 1994, A&A 288, 738-745

Baity W.A., Rothschild R.E., Lingenfelter R.E., et al., 1981, ApJ 244, 429-435

von Ballmoos P., Diehl R., Schönfelder V., 1987, ApJ 312, 134-142

Bloemen H., Hermsen W., Swanenburg B.N., et al., 1994, ApJS 92, 419-423

de Boer H., Bennett K., Bloemen H., et al., 1992, Maximum Likelihood Method Applied to COMPTEL Source Recognition and Analysis. In: Di Gesu V., Scarsi L., Buccheri R., et al. (eds.) Data Analysis in Astronomy IV. Plenum, New York, Vol. 59, pp. 241-249

Bond I.A., Ballet J., Denis M., et al., 1996, A&A 307, 708-714

Dermer C.D., Gehrels N., 1995, ApJ 447, 103-120

Dermer C.D., Schlickeiser R., 1993, ApJ 416, 458-484

Ebneter K., Balick B., 1983, PASP 95, 675-690

Feigelson E.D., Schreier E.J., Devaille J.P., et al., 1981, ApJ 251, 31-51

Fichtel C.E., Bertsch D.L., Chiang J., et al., 1994, ApJS 94, 551-581

Gehrels N., Cheung C., 1992, High Energy Continuum Measurements of Active Galactic Nuclei. In: Holt S.S., Neff S.G., Urry C.M. (eds.) Testing the AGN Paradigm, AIP Conf. Proc. 254, pp. 348-355

Hall R.D., Meegan C.A., Walraven G.D., Djuth F.T., Haymes R.C., 1976, ApJ 254, 631-641

Harris G.L.H., Hesser J.E., Harris H.C., Curry P.J., 1984, ApJ 287, 175-184

den Herder J.W., Aarts H., Bennett K., et al., 1992, COMPTEL Processing and Analysis Software System COMPASS. In: Di Gesu V., Scarsi L., Buccheri R., et al. (eds.) Data Analysis in Astronomy IV. Plenum, New York, Vol. 59, pp. 217-228

Hui X., Ford H.C., Ciardullo R., Jacoby G.H., 1993, ApJ 414, 463-473

Johnson W.N., Dermer C.D., Kinzer R.L., et al., 1995, ApJ 445, 182-188

Jones D.L., Tingay S.J., Murphy D.W., et al., 1996, ApJ 466, L63-L65

Jourdain E., Bassani L., Roques J.P., et al., 1993, ApJ 412, 586-592

Kinzer R.L., Johnson W.N., Dermer C.D., et al., 1995, ApJ 449, 105-118

Lampton M., Margon B., Bowyer S., Mahoney W., Anderson K., 1972, ApJ 171, L45-L50

Lampton M., Margon B., Bowyer S., 1976, ApJ 208, 177-190

Lichti G.G., Balonek T., Courvoisier T.J.L., et al., 1995, A&A 298, 711-725

Maisack M., Kendziorra E., Mony B., et al., 1992, A&A 262, 433-440

Marcowith A., Henri G., Pelletier G., 1995, MNRAS 277, 681-699

McNaron-Brown K., Johnson W.N., Jung G.V., et al., 1995, ApJ 451, 575-584

Morganti R., Fosbury R.A.E., Hook R.N., Robinson A., Tsvetanov Z., 1992, MNRAS 256, 1P-5P

Morini M., Anselmo F., Molteni D., 1989, ApJ 347, 750-759

Nolan P.L., Bertsch D.L., Chiang J., et al., 1996, ApJ 459, 100-109

Paciesas W.S., Harmon B.A., Pendleton G.N., et al., 1993, A&AS 97, 253-255

Schönfelder V., Aarts H., Bennett K., et al., 1993, ApJS 86, 657-692

Simpson G., Mayer-Hasselwander H., 1986, A&A 162, 340-348

Skibo J.G., Dermer C.D., Kinzer R.L., 1994, ApJ 426, L23-L26

Steinle H., Bloemen H., Collmar W., et al., 1993, Adv. Space Res. Vol. 13, No.12, pp. 731-734

Stocke J.T., Morris S.L., Gioia I., et al., 1990, ApJ 348, 141-146

Strong A.W., Cabeza-Orcel P., Bennett K., et al., 1992, Maximum Entropy Imaging and Spectral Deconvolution for COMPTEL. In: Di Gesu V., Scarsi L., Buccheri R., et al. (eds.) Data Analysis in Astronomy IV. Plenum, New York, Vol. 59, pp. 251-260

Strong A., Diehl R., Oberlack U., et al. 1997, Whole Sky Maps Using 5 Years of COMPTEL Data. In: Winkler C., Courvoisier T.J.-L., Dorouchoux Ph. (eds.) Proc. 2nd INTEGRAL Workshop, The Transparent Universe. ESA SP-382, pp. 533-536

Terrell J., 1986, ApJ 300, 669-674

Thompson D.J., Bertsch D.L., Dingus B.L., et al., 1995, ApJS 101, 259-286

Urry M.C., Padovani P., 1995, PASP 107, 803-845

This article was processed by the author using Springer-Verlag LaTeX A&A style file *L-AA* version 3.